


Temperature dependence of the Gilbert damping of $\text{La}_{0.7}\text{Sr}_{0.3}\text{MnO}_3$ thin films

Victor Haspot,¹ Paul Noël^{1,2,*}, Jean-Philippe Attané,² Laurent Vila,² Manuel Bibes¹, Abdelmadjid Anane,¹ and Agnès Barthélémy¹

¹*Unité Mixte de Physique, CNRS/Thales, Université Paris-Saclay, 91767 Palaiseau, France*

²*Université Grenoble Alpes, CEA, CNRS, Grenoble, INP, IRIG-Spintec, Grenoble, France*

 (Received 30 June 2021; revised 20 September 2021; accepted 8 December 2021; published 22 February 2022)

Due to its half metallic nature, $\text{La}_{0.7}\text{Sr}_{0.3}\text{MnO}_3$ is an attractive highly correlated electronic system to obtain ultralow magnetic damping. In this paper we analyze the temperature and thickness dependence of the damping of the magnetization dynamic of epitaxial thin $\text{La}_{0.7}\text{Sr}_{0.3}\text{MnO}_3$ films. Our analysis reveals that the damping encompasses resistivelike and conductivelike contributions, as in transition metal ferromagnets. The data also show a large increase of the ferromagnetic resonance linewidth at low temperature, a feature that we ascribe to the presence of a dead layer, insulating and magnetically active, that behaves like a spin sink. The associated spin-pumping term shows a strong temperature dependence, linked to that of the spin mixing conductance. By clarifying some unexplored aspects of spin dynamics in half-metallic manganites, our results contribute to the progress in the burgeoning field of oxide spin orbitronics.

DOI: [10.1103/PhysRevMaterials.6.024406](https://doi.org/10.1103/PhysRevMaterials.6.024406)

I. INTRODUCTION

Materials with ultralow magnetic damping are of primary importance in the framework of spintronics, to produce fast and energy-efficient spintronic devices such as spin transfer torque magnetic random access memories (MRAMs), nano-oscillators or low-loss materials for magnonics. The development of spintronics based on oxides, i.e., spin oxitronics, has been accelerating in the past years, with several important milestones achieved such as record of magnetoresistance in magnetic tunnel junctions with half metallic electrodes [1] or the discovery of a highly efficient spin-charge interconversion [2] in two-dimensional high-mobility electron gas appearing at oxide interfaces [3]. Together with the multiferroic-based voltage control of the magnetization [4], the voltage control of the spin-charge interconversion [5], and the development of ferroelectric [6] or multiferroic [7,8] tunnel junctions, this provides a platform to develop oxide-based spintronics applications.

In this context, the damping of ferromagnetic oxides is a key issue. In magnetic systems damping governs the relaxation of the magnetization dynamics through the Landau Lifshitz-Gilbert equation [9,10]: $\frac{d\vec{M}}{dt} = -\gamma\vec{M} \times \vec{H}_{\text{eff}} - \frac{\alpha}{M_s}\vec{M} \times \frac{d\vec{M}}{dt}$, where \vec{M} is the magnetization vector, \vec{H}_{eff} is the effective magnetic field acting on \vec{M} , γ is the gyromagnetic ratio, M_s is the saturation magnetization, and α is the Gilbert damping coefficient. Half metals are particularly attractive materials due to their 100% spin polarization and predicted related ultralow damping [11], which has for instance been exemplified by the very low effective damping of Heusler alloys (7×10^{-4}) [12].

$\text{La}_{0.7}\text{Sr}_{0.3}\text{MnO}_3$ (LSMO) is another promising half metal with a Curie temperature (360 K) above room temperature. Its half-metallic character has been evidenced through spin polarized photoemission experiments [13] and record-high tunnel magnetoresistance in magnetic tunnel junctions with LSMO electrodes [1]. An ultralow damping has been reported for this compound (5.2×10^{-4}) for 44.6-nm-thick films grown on $\text{NdGaO}_3(110)$ [14], but to the best of our knowledge the temperature dependence of the Gilbert damping has not been studied yet. Due to the very strong temperature dependence of its resistivity, with a residual resistivity ratio (RRR) of 10–15, temperature should strongly influence the damping, as previously observed for other ferromagnets [15].

We report here the temperature dependence of the Gilbert damping parameter of LSMO films grown on (001) oriented single crystals of $(\text{LaAlO}_3)_{0.3}(\text{Sr}_2\text{AlTaO}_6)_{0.7}$ (LSAT), with thicknesses in the 5.6 to 16.5 nm range. Surprisingly, despite the half metallic nature of the LSMO, at low temperature the damping coefficient is larger than at room temperature, with a peak around 30 K, in line with results obtained in FM/AFM heterostructures [16,17]. We analyze the temperature dependence of the damping of LSMO by considering resistivelike and conductivelike contributions, and an additional term due to spin pumping related to the presence of a magnetically active dead layer. This latter term presents a pronounced temperature dependence, linked to the coupling of the magnetic moment of the active part of the layer with spins in the magnetic-insulating portion, and to the large variation in temperature of the resistivity that results in more localized electrons in the conductive part of the layer.

II. METHODS

LSMO films were grown by pulsed laser deposition on (001) oriented single crystals $(\text{LaAlO}_3)_{0.3}(\text{Sr}_2\text{AlTaO}_6)_{0.7}(001)$ (LSAT) using a KrF laser with

*Present address: Department of Materials, ETH Zürich, Hönggerberg 64, 8093 Zürich, Switzerland.

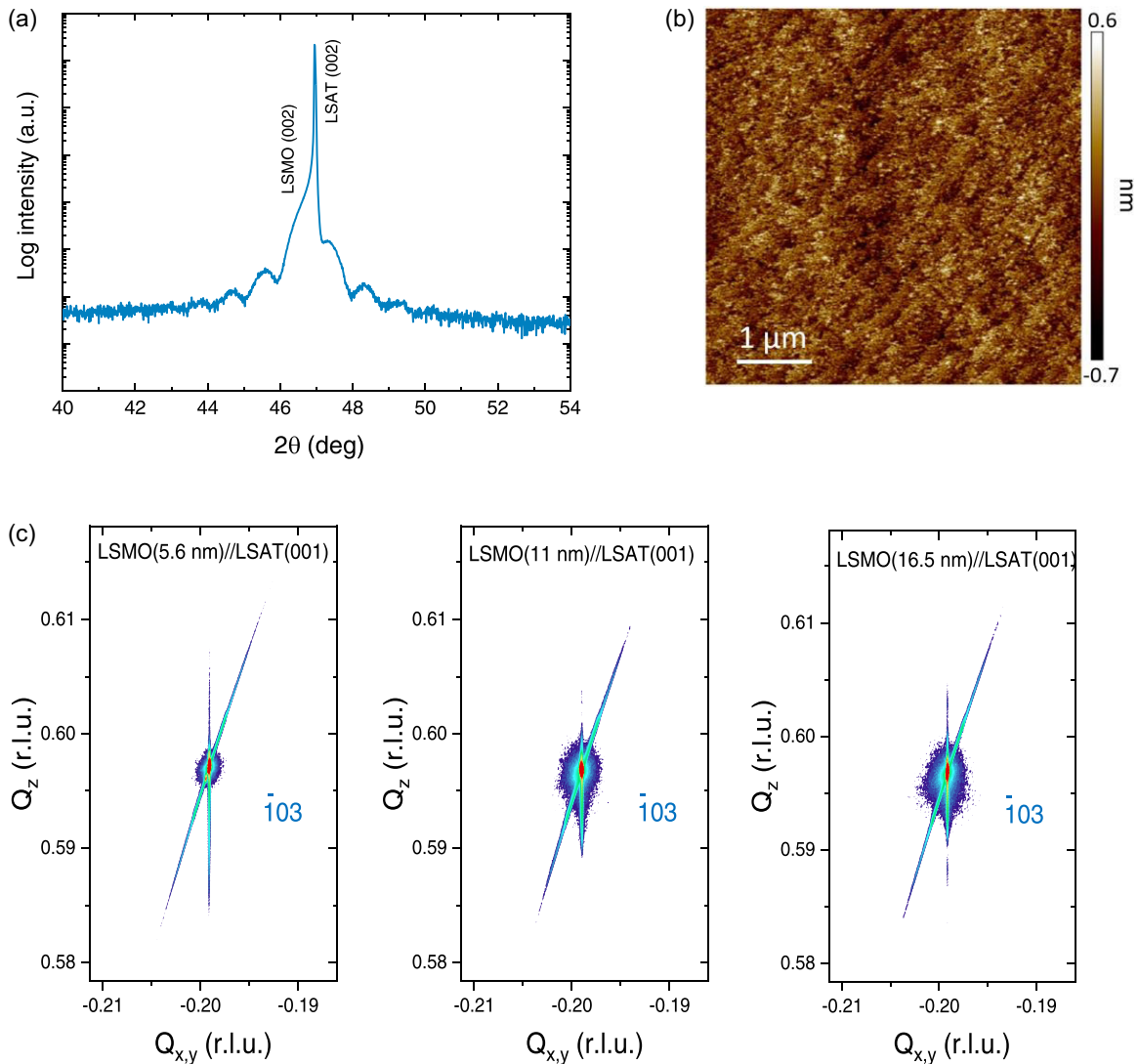


FIG. 1. (a) θ - 2θ scan around the (002)-pc peak of the 11-nm LSMO film. (b) Atomic force microscopy characterization of the film. (c) Reciprocal space maps around the (103) reflections for different thicknesses of the LSMO films (r.l.u. stands for relative lattice units).

a 248-nm wavelength. The films were grown at 2 Hz, under an oxygen pressure of 0.2 mbar and a temperature of 800 °C. After deposition the films were annealed half an hour at 650 °C under 200 mbar, and then cooled to room temperature at a rate of 20 °C per minute under the same pressure. The film thickness was monitored using reflexion high energy electron diffraction oscillations and controlled by x-ray reflectometry. The crystalline structure was characterized by x-ray diffraction and reciprocal space maps. The magnetic and transport properties were characterized by a superconducting quantum interference device (SQUID) and a physical property measurement system (PPMS). We measured the ferromagnetic resonance (FMR) response at different frequencies from 2 to 18 GHz, using a broadband coplanar waveguide and magnetic field modulation.

III. RESULTS AND DISCUSSION

A series of LSMO thin films ranging from 5.6 to 16.5 nm in thickness was grown. Figure 1(a) shows a typical θ - 2θ

scan around the (002)-pc peaks of a 11 nm LSMO (pc standing for pseudocubic). Laue fringes suggest a good structural coherence and a smooth surface, confirmed by atomic force microscopy images [see Fig. 1(b)]. Reciprocal space maps [Fig. 1(c)] revealed that films up to 16.5 nm are fully strained.

The temperature and field dependence of the magnetization for the different films are presented in Figs. 2(a)–2(c). The magnetization easy axis is [110] for all films [see Fig. 2(a)] in good agreement with literature [18]. The in-plane magnetocrystalline anisotropy parameter K_1 deduced from these curves is 2 mJ/cm³, corresponding to an out-of-plane anisotropy field of $\mu_0 H_A = 745$ mT, in line with previously reported values [18] for LSMO on LSAT, and thus pointing towards similar strain and magnetoelastic constants. The observed reduction of the saturation magnetization M_S and of the Curie temperature T_C observed when thickness decreases [Figs. 2(b) and 2(c)] are also consistent with the literature [19,20]. Whereas $M_S = 582$ emu/cm³ for the thicker films at low temperature, it is reduced to 427 emu/cm³ when the film thickness is 5.6 nm. Such a reduction is generally as-

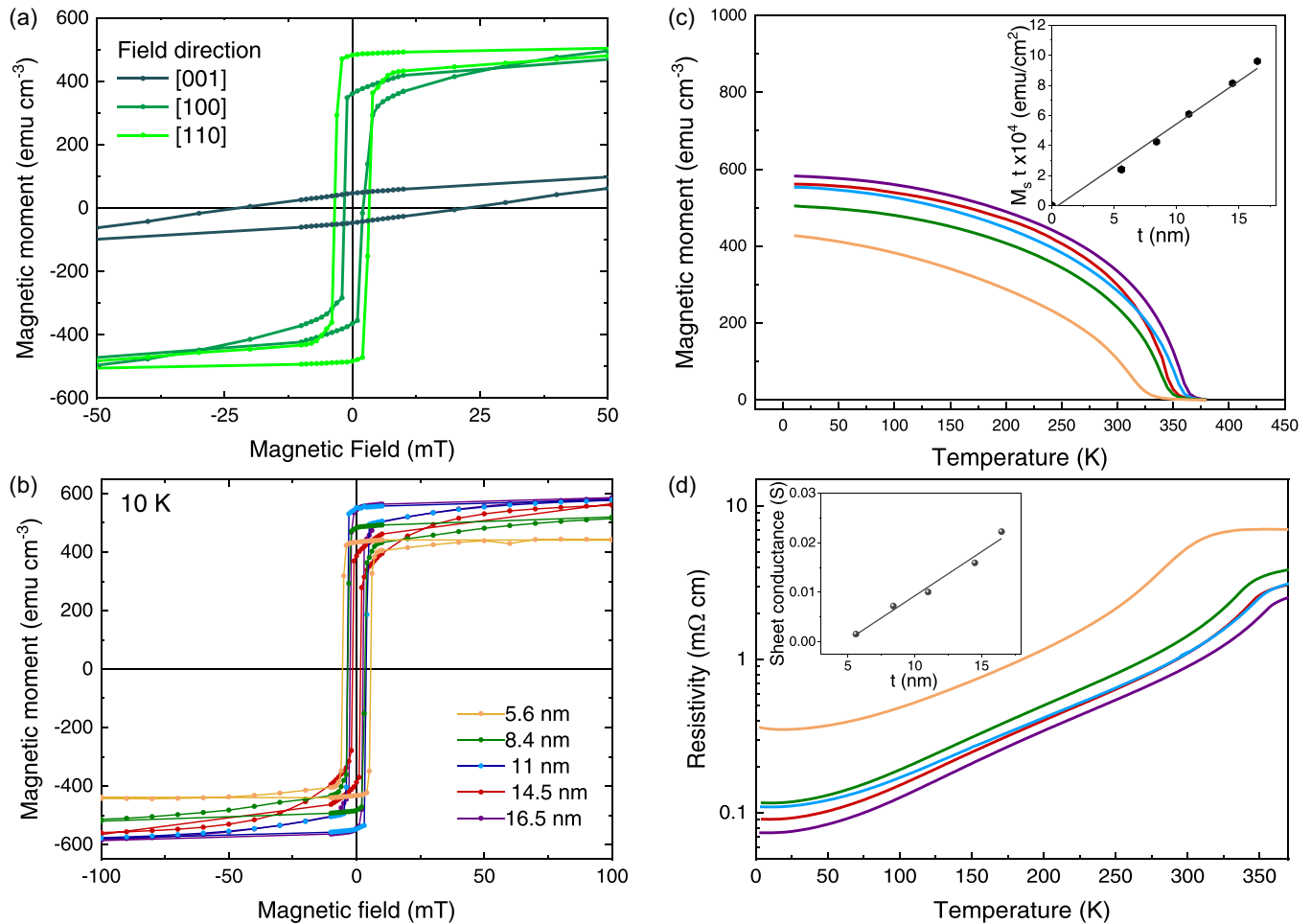


FIG. 2. (a) Magnetic hysteresis loops at 10 K of the 8.4-nm film along different directions. (b) Hysteresis loops of the films measured along the [110] direction for films with different thicknesses. (c) Temperature dependence of the magnetization (at 100 mT) of the films. The inset is the thickness dependences of the 10-K magnetization, fitted with a simple bilayer model. (d) Temperature dependence of the resistivity of the films. The inset is the thickness evolution of the sheet conductance at 10 K and the linear fit. For (b)–(d) the symbol colors are orange, green, blue, red, and violet for the 5.6-, 8.4-, 11-, 14.5-, and 16.5-nm films, respectively.

cribed to the presence of a “dead layer” or of a magnetic layer with decreased magnetism at the surface or interface with the substrate. Such difference between the bulk and the surface/interface associated with the weakening of the double exchange mechanism in manganite has been attributed to surface segregation [21,22], a change in the Mn valence [23], modified orbital occupancy, and/or oxygen octahedron tilting related to symmetry breaking [24].

The temperature dependence of the resistivity is presented in Fig. 2(d). The residual resistivity at 10 K is in the 75–360- $\mu\Omega\text{-cm}$ range, in agreement with previously reported values [20]. When the LSMO layer thickness decreases, the resistivity increase indicates the presence of a layer with reduced conductivity due to a weakened double exchange at surface/interface. This appears more clearly in the thickness dependence of the film total conductance G_{\square} at 10 K, defined as $G_{\square} = 1/R_{\square}$ where R_{\square} is the sheet resistance at 10 K, and presented in the inset of Fig. 2(d) [25]. A thickness of the nonmetallic layer of about 4.8 nm can be deduced, in good agreement with the value of 3.2 or 4 nm previously reported for LSMO films on SrTiO₃ (001) [26], considering the slight compressive strain

imposed by the LSAT substrate promoting a reduced double exchange. Taking into account this dead layer thickness, it is possible to fit the dependence of the measured saturation magnetization M_s with the thickness t [see inset of Fig. 2(c)] considering a simple bilayer model, i.e., $M_s t = M_B(t - t_{DL}) + M_{DL}t_{DL}$ with M_B the saturation magnetization of the bulklike layer, M_{DL} the saturation magnetization of the dead layer and t_{DL} its thickness. In that case, the best agreement is found for $M_B = (570 \pm 20)$ emu/cm³ and $M_{DL} = (512 \pm 26)$ emu/cm³, whereas considering a dead layer with a zero magnetization and whose thickness is a free parameter, one finds $t_{DL} = (0.5 \pm 0.3)$ nm [right inset of Fig. 2(c)].

The typical dynamic magnetic responses of our samples using ferromagnetic resonance (FMR) at room temperature are presented in Figs. 3(a)–3(c) (here, for a film thickness of 16.5 nm). Figure 3(a) displays the field derivative of the imaginary part of the dynamic magnetic susceptibility χ'' for different frequencies f of the microwave excitation, as a function of the applied magnetic field H_{dc} . The corresponding frequency dependence of the resonance field H_{res} and of the peak-to-peak linewidth ΔH_{pp} are reported in Figs. 2(b) and 2(c) respectively. The dispersion

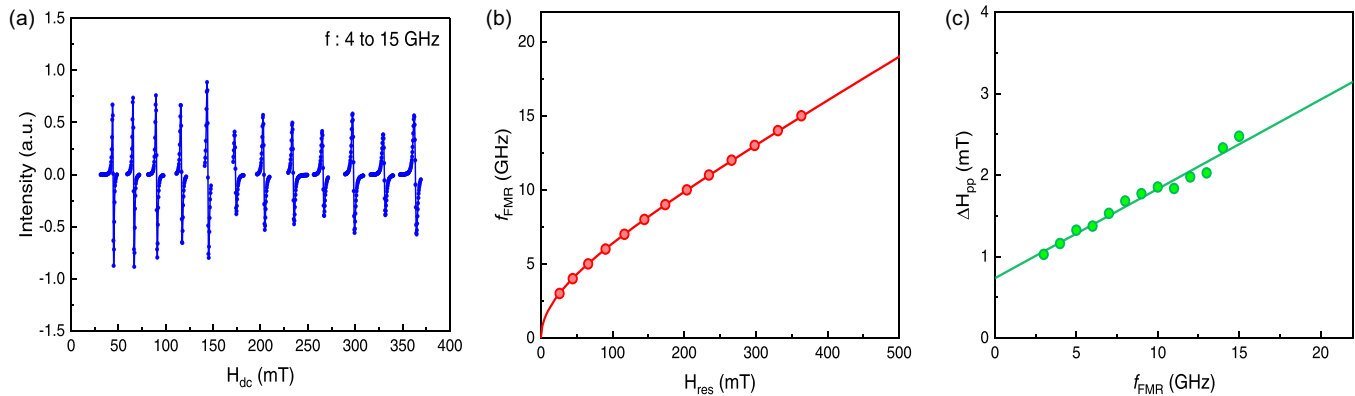


FIG. 3. Dynamic magnetic response at room temperature of the LSMO 16.5 nm/(001)LSAT measured along the 110 axis: (a) imaginary part of the dynamic susceptibility χ'' for different frequencies f of the microwave excitation (steps of 1 GHz), as a function of the applied magnetic field H_{dc} . (b) Resonance frequency f_{FMR} as function of the resonance field H_{res} . The fit corresponds to Kittel's law. (c) Evolution of peak-to-peak linewidth ΔH_{pp} (symbol) with the resonance frequency. The Gilbert damping extracted by fitting.

relation of H_{res} with f [Fig. 3(b)] follows the Kittel's law [27], $f = \mu_0 \frac{g\mu_B}{h} \sqrt{(H_{\text{res}} + H_{\text{R}})(H_{\text{res}} + H_{\text{R}} + M_{\text{eff}})}$ with M_{eff} the effective magnetization, H_{R} the anisotropy field, and g the effective electron g factor, taken to be 2.01. The effective Gilbert damping α_{LSMO} was determined by fitting the frequency dependence of the peak-to-peak linewidth ΔH_{pp} [Fig. 3(c)], with $\Delta H_{\text{pp}}(f) = \Delta H_0 + \frac{2}{\sqrt{3}} \left(\frac{2\pi f}{g\mu_B} \right) \hbar \alpha_{\text{LSMO}}$ where ΔH_0 is the frequency independent contribution arising from magnetic inhomogeneities in the LSMO film. The effective damping is $(2.63 \pm 0.01) \cdot 10^{-3}$ for this 16.5-nm film at room temperature, slightly larger than values reported in the literature for thicker LSMO films on LSAT (7.4×10^{-4} [14]; $9 \cdot 10^{-4}$ [28]) or SrTiO_3 (1.5×10^{-3} [29,30]). This value is comparable to that of the transition metal alloys with the lowest damping [31] [FeV (2×10^{-3}), CoFe (2.1×10^{-3})] and of Heusler alloys as CoFeGe (2.18×10^{-3}) [32]. Moreover, the inhomogeneous broadening is low, evidencing the good homogeneity of the film.

The temperature dependence of the effective Gilbert damping α_{LSMO} is presented in Fig. 4(a). At room temperature the damping is not particularly affected by the thickness, except for the 5.6-nm sample. The increase of the damping in thin films is usually ascribed to electron-electron scattering at surface/interface [14] or surface/interface imperfection/scatterers inducing local variations in resonance field or to two-magnon scattering [33]. In the case of LSMO the large enhancement only for the thinnest film is likely due to the vicinity of the Curie temperature [34], as the Curie temperature is lower for the 5.6 nm (325 K) compared to thicker films (more than 350 K). As the temperature increases, α presents a maximum around 20–30 K whose amplitude increases at smaller thickness, decreases up to 150–250 K depending on the film thickness, and finally shows an upturn upon approaching T_{C} . Such an unexpected and unusual enhancement of the damping at low temperature has been also observed for transition metal ferromagnets such as Fe [15] or for the ferrimagnetic insulator YIG [35] and attributed to either intraband scattering or relaxation mechanisms.

To account for these temperature dependencies, we discarded extrinsic contributions related to the dissipation of energy due to eddy currents, that can be estimated to

10^{-7} (10^{-6}) for the thinner (thicker) film. We can also safely rule out the scattering of the uniform precession with short wavelength magnons due to roughness and/or inhomogeneities, since the magnetization is almost constant in the 5–100-K range and that a similar linewidth is measured when the field is applied out of plane (not shown), a configuration where the two-magnon scattering is considered inefficient [36].

The Gilbert damping is ascribed to the dissipation of the energy of the magnetic system towards the lattice promoted by spin-orbit coupling [37]. In the case of ferromagnetic transition metals, temperature dependencies of the Gilbert damping showing a similar minimum have been interpreted theoretically and experimentally by considering two contributions, i.e., adding a conductivelike to a resistivelike term [38–40]. In Kambersky's torque correlation model [39], the first term, also called the intraband term, is typically understood through the breathing Fermi surface model, where spin-orbit-induced electron-hole pairs created in the same band close to the Fermi level by the magnetization dynamics relax to the lattice. The damping by this mechanism increases linearly with the electronic momentum scattering time τ yielding a “conductivitylike” Gilbert damping. In contrast, the interband scattering mechanism where magnetization dynamics excites electron-hole pairs across different bands corresponds to a Gilbert damping proportional to $1/\tau$ and scales with the resistivity.

To account for the temperature dependence of α_{LSMO} , we simulated our experimental curves considering two adding terms—a conductivelike and resistivelike one [38,15]—using the transport properties presented in Fig. 2(d):

$$\alpha_{\text{LSMO}} = \alpha_{\text{intra}} \frac{\sigma(T)}{\sigma(300 \text{ K})} + \alpha_{\text{inter}} \frac{\rho(T)}{\rho(300 \text{ K})}.$$

The conductivelike term, also called the intraband term, and the resistivelike term, likewise referred to as the interband term, are related to spin- \uparrow to spin- \downarrow transitions allowed by the temperature. Indeed, whereas LSMO is a half metal at very low temperature [13] due to the hole transfer (e_g band of $d_{x^2-y^2}$ and d_{z^2} character) from Mn^{4+} to Mn^{3+} through the

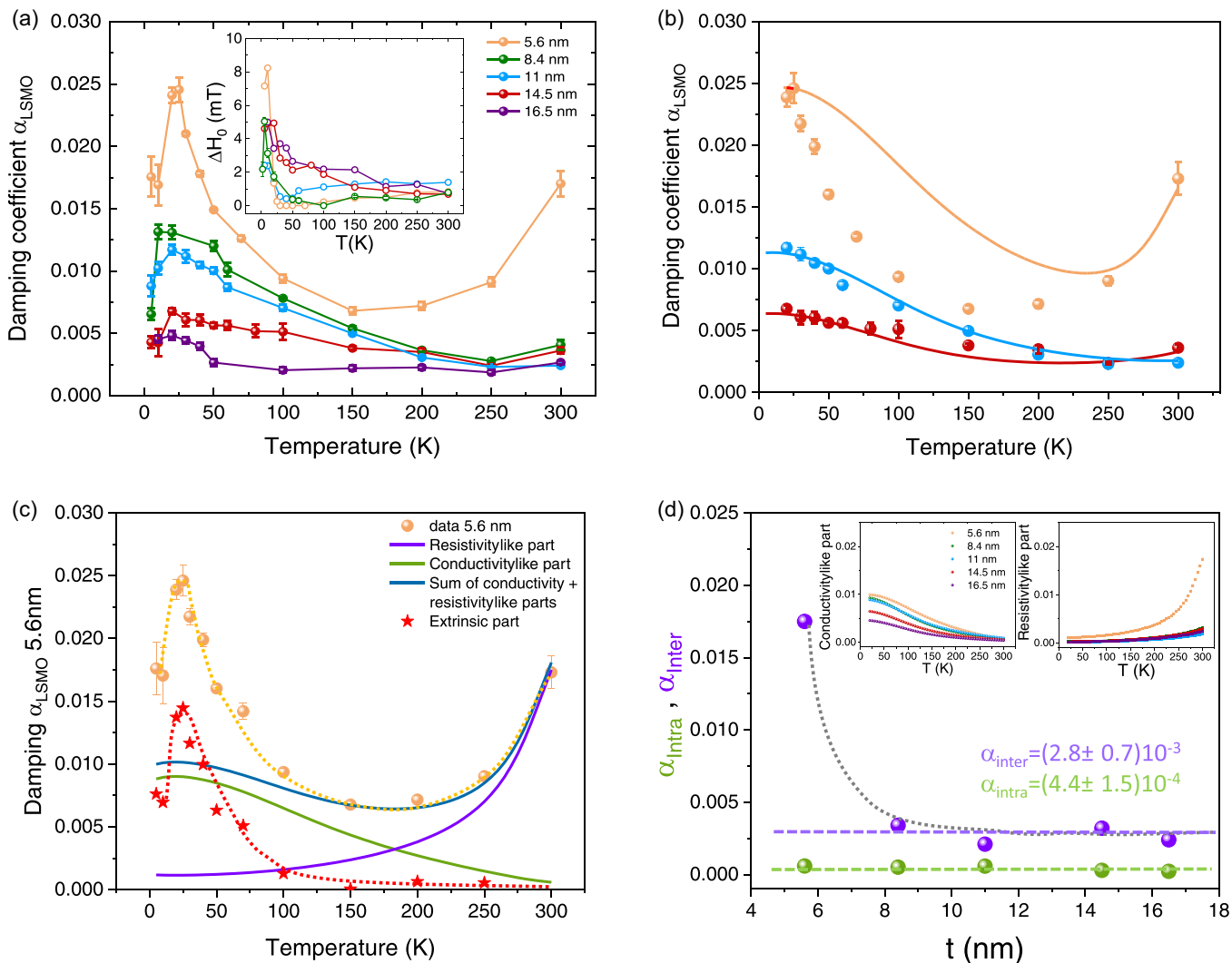


FIG. 4. (a) Temperature dependence of the Gilbert damping term for films with different thicknesses. Inset: temperature dependence of ΔH_0 . (b) Simulation of the temperature dependence of the damping. Symbols correspond to the experimental results, and lines to the sum of conductivitylike and resistivitylike contributions. (c) Temperature dependence of the damping of the 5.6-nm LSMO film. Green and violet lines are the conductivitylike (α_{intra}) and resistivitylike (α_{inter}) contributions and the blue line is their sum. The red symbols correspond to the additional term α_{ext} . (d) Thickness dependence of α_{inter} and α_{intra} . Left (right) inset is the conductivitylike (respectively, resistivitylike) contribution.

oxygen atom possible when the magnetic moments of the core spins are parallel (localized t_{2g} of d_{xz} , d_{yz} , or d_{xy} character), the temperature induces a misalignment of the t_{2g} magnetic moments which affects the hole hopping resulting in a lowering of the double exchange and the related loss of the half metallic character [41]. In Fig. 5, we illustrate this mechanism. At very low temperature [Fig. 5(a)], all the t_{2g} magnetic moments are aligned defining a common quantization axis. The band structure is composed of a filled $t_{2g\uparrow}$ band, a partially filled $e_{g\uparrow}$ band (0.3 holes) and empty $t_{2g\downarrow}$ and $e_{g\downarrow}$ bands. When temperature increases, the misalignment of the t_{2g} magnetic moments affects the hopping of the e_g holes from site to site inducing the lowering of the double exchange and the presence of spin and spin down states at the Fermi level. In Figs. 5(b) and 5(c), we illustrate this case considering two sites (A in red and B in blue) with an angle θ (for simplicity we consider that $\phi = 0$) between their localized t_{2g} magnetic

moments. The reference quantization axis is defined by the direction of the magnetic moment on the A site. In this reference frame, the magnetic moment on site B ($|\nearrow$) decomposed as $|\nearrow\rangle = \cos(\theta/2)|\uparrow\rangle + \sin(\theta/2)|\downarrow\rangle$ inducing the presence of a spin- \downarrow band at the Fermi level with a density of state that increases as the angle θ increases [which is represented for $\theta = 60^\circ$ and 90° in Figs. 5(b) and 5(c) respectively]. Note that since the hopping of the e_g hole that varies as $\cos(\theta/2)$ is smaller at temperature T than at $T = 0$ it results in more localized e_g bands. To account for the paramagnetic-insulating state it is enough to consider that $\theta = 180^\circ$ and that the insulator character is induced by the decrease of the e_g bandwidth [42]. The presence at the Fermi level of spin- \uparrow and spin- \downarrow states allows $d_{z^2\uparrow}$ to $d_{z^2\downarrow}$ or $d_{x^2-y^2\uparrow}$ to $d_{x^2-y^2\downarrow}$ (and vice versa) transitions giving rise to an intraband term and to $d_{z^2\uparrow}$ to $d_{x^2-y^2\downarrow}$ or $d_{x^2-y^2\uparrow}$ to $d_{z^2\downarrow}$ (and vice versa) transitions resulting in an interband contribution to the damping.

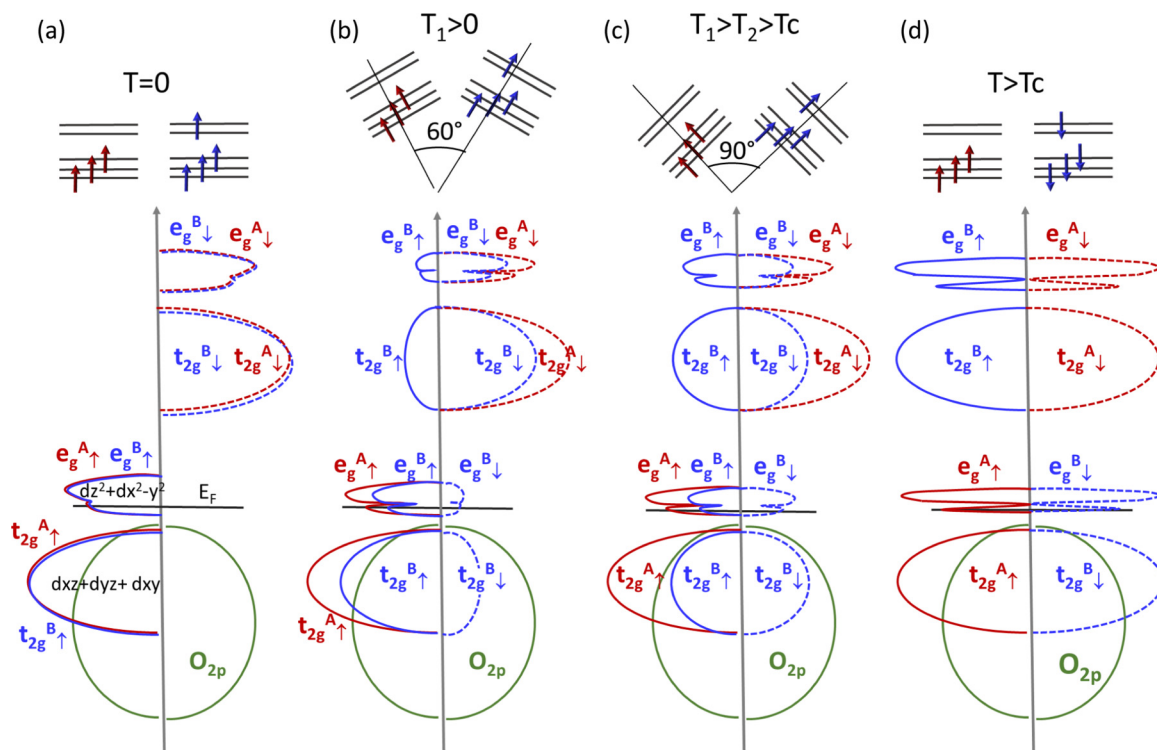


FIG. 5. Schematic of the band structure of LSMO at different temperatures. (a) At $T = 0$ K, t_{2g} magnetic moments of all atoms are parallel allowing a maximum hopping of the e_g hole resulting in half metallicity with only spin \uparrow states at the Fermi level. (b), (c) When T increases, it induces a canting between t_{2g} magnetic moments resulting in a decreased double exchange together with the presence of spin- \uparrow and spin- \downarrow states at the Fermi level, i.e., a loss of the half metallic character and the opportunity for spin- \uparrow (\downarrow) to spin- \downarrow (\uparrow) transitions that increase the damping via conductivelike and resistivelike contributions. (d) Above the Curie temperature, T_C , LSMO is in the paramagnetic insulating state.

We show in Fig. 4(b) fits of the data for three samples above 30 K. Whereas the agreement between the data and this simple model is quite good for the thicker films it is not the case for the thinnest one. The decrease of the damping below 30 K cannot be explained by considering only resistivitylike and conductivitylike contributions. To fully account for the experimental data, we thus consider not only a resistivelike and a conductivitylike terms, but also an additional extrinsic term α_{ext} , and simulate the data with $\alpha_{\text{LSMO}} = \alpha_{\text{intra}} \frac{\sigma(T)}{\sigma(300\text{K})} + \alpha_{\text{inter}} \frac{\rho(T)}{\rho(300\text{K})} + \alpha_{\text{ext}}$. Figure 4(c) presents the conductive (green), resistive (violet), and extrinsic (red) contributions to the damping of the 5.6-nm film. While above about 100 K, the data are dominated by the resistivelike and conductivitylike term, the extrinsic term becomes prominent at low temperature and shows a maximum near 30 K.

The extracted conductivitylike contribution $\alpha_{\text{LSMO}} = \alpha_{\text{intra}} \frac{\sigma(T)}{\sigma(300\text{K})}$ to the damping evolution in temperature is presented in the left inset of Fig. 4(d). It corresponds to a small and almost thickness independent $\alpha_{\text{intra}} = (4.4 \pm 1.5) 10^{-4}$, in good agreement with the half-metallic nature of LSMO at low temperature [see left inset of Fig. 4(d)]. The interband term contribution $\alpha_{\text{inter}} \frac{\rho(T)}{\rho(300\text{K})}$ is shown in the right inset of Fig. 4(d). This term varies as $1/\tau$ and has a prominent variation for the thinner film due to its depressed Curie temperature. Except for the thinnest film α_{inter} is independent of the film thickness with $\alpha_{\text{inter}} = (2.8 \pm 0.7) 10^{-3}$ [see Fig. 4(d)].

We now discuss the possible origin of the term α_{ext} , whose contribution to the evolution of total damping in temperature is presented in Fig. 6(a) for the different films. This term only has a significant contribution below 100 K, and its contribution to the total damping increases while the thickness decreases. The inset of Fig. 6(a) presents the dependence of the maximum value of α_{ext} with $1/M_s(t - t_{\text{DL}})$. The observed $1/M_s(t - t_{\text{DL}})$ variation points towards spin pumping by the magnetically active insulating “dead layer,” which would thus act as a spin sink. The fit of α_{ext} at maximum by $g_{\uparrow\downarrow} \frac{\mu_{\text{B}} g}{4\pi} \frac{1}{M_s(t - t_{\text{DL}})}$ leads to a spin-mixing conductance $g_{\uparrow\downarrow}$ of 19 nm^{-2} . This large value, similar to those observed for metallic interfaces [43–45], is consistent with the continuity of the oxygen octahedral network through the interface between the active layer and the insulating one, promoting a high transparency. The spin mixing conductance appears to be temperature dependent and in particular increases substantially at low temperatures.

A comparable temperature dependence of the damping due to spin pumping into an adjacent layer has been reported for NiFe/NiFeOx and NiFe/IrMn [16,17,46], and ascribed to spin injection from the exchange-biased ferromagnetic NiFe layer in the neighboring antiferromagnetic insulator, which undergoes an antiferromagnetic to paramagnetic transition. As shown in Fig. 6(b), and similarly to the NiFe/IrMn and NiFe/NiFeOx cases, at low temperature the resonance fields of LSMO films significantly depart from Kittel’s law with no

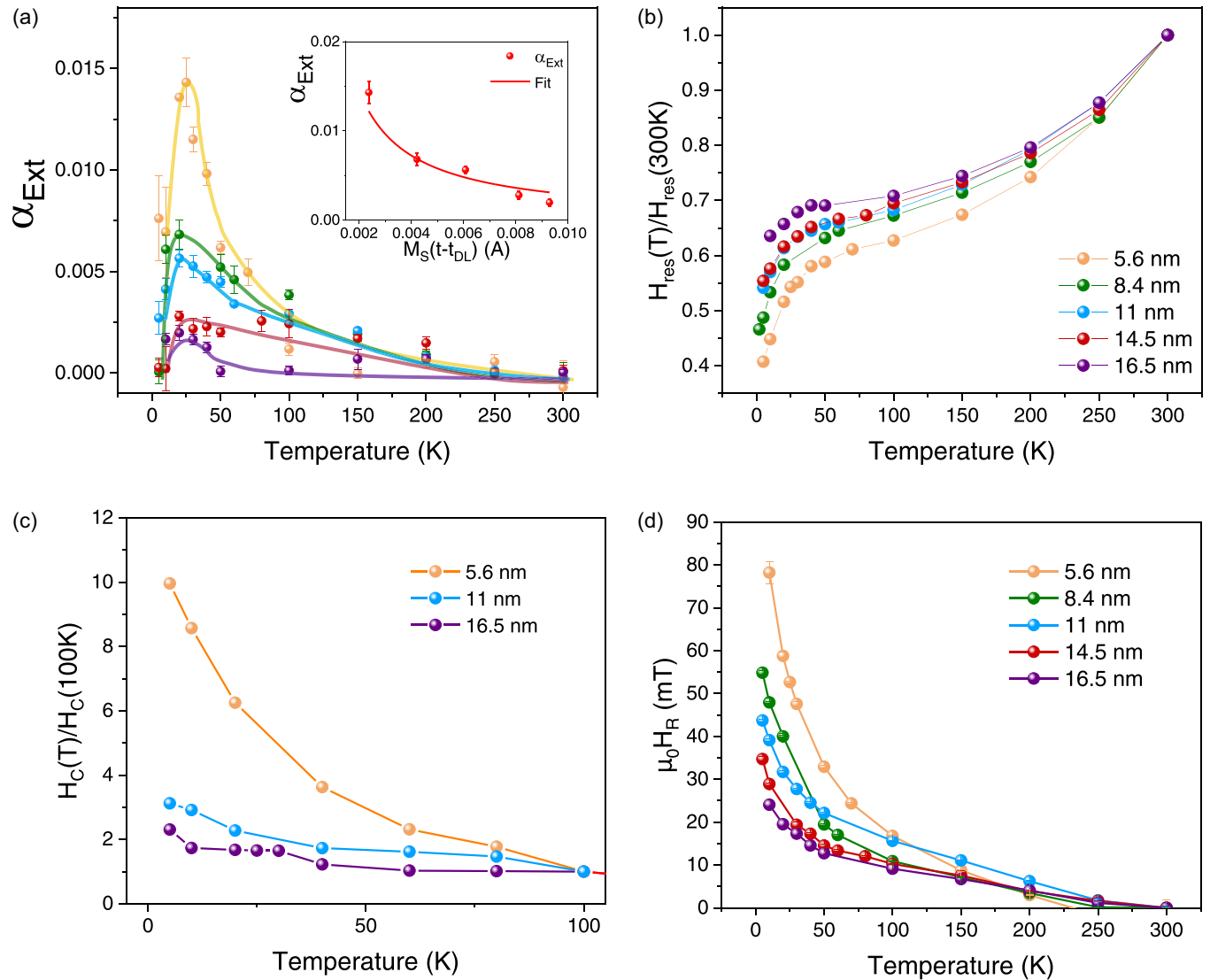


FIG. 6. (a) Extrinsic contribution α_{Ext} to the damping for the different LSMO films, lines are guides for the eyes. Inset: Plot (symbol) and fit (line) of the maximum of α_{Ext} vs $M_S(t - t_{\text{DL}})$. (b) Evolution of the resonance field with the temperature. (c) Evolution of the coercive field as a function of temperature. (d) Temperature dependence of the rotational anisotropy field H_R .

additional anisotropy field H_R . In our case we do not observe any shift of the hysteresis loop linked to an exchange bias due to exchange coupling between pinned uncompensated spins in the antiferromagnet and ferromagnetic moments. We nevertheless see a clear increase of the coercive field at low temperature [see Fig. 6(c)] that is generally attributed to some coupling between unpinned uncompensated spins in the antiferromagnet and ferromagnet magnetic moments at the interface [47]. The presence in LSMO films at the surface or at the interface with the substrate of a canted-ferromagnetic insulating layer [48–50] or a layer with phase separation [51] due to the lowering of the double exchange mechanism is a well-known phenomenon leading to an insulating layer with poor magnetic properties [52]. Since the enhancement of the damping by spin fluctuations applies to all kinds of ordering and electrical states, regardless of the electronic or magnonic nature of the spin current probe [46], a possible scenario could be related to the presence of this canted-ferromagnetic insulating or phase-separated layer resulting in a magnetically active

insulating layer with shorter spin relaxation time coupled to the ferromagnetic part of the film. The spin fluctuations in the magnetically active dead layer acting as a spin sink lead to an enhancement of the damping of the ferromagnetic portion of the film coupled to it. Due to its uncontrolled nature this layer and the induced anisotropy are likely to be spatially inhomogeneous. This is a possible cause for the enhancement of the inhomogeneous broadening ΔH_0 at intermediate temperature (30–100 K) as seen in the inset of Fig. 4(a). Those fluctuations tend to freeze at the lowest temperature, below 25–30 K [50], a behavior which is reminiscent of a disorder induced spin-glass transition therefore suppressing spin relaxation channels. As a result the relaxation (damping α and ΔH_0) decreases.

The coupling between the magnetic moments in the ferromagnetic metallic part of the LSMO layer to the spins of this magnetically active insulating layer alters the resonance field and results in an additional rotational anisotropy H_R in Kittel's formula [53,47]. The temperature dependence of H_R reported in Fig. 6(d) is very similar to what was observed

for the NiFe/IrMn system [17]. It corresponds to a dynamic interfacial exchange constant $J_{\text{Dyn}} = \mu_0 H_R(T) M_s(T) (t - t_{\text{DL}})$ of (0.21 ± 0.03) mJ/m² at 10 K, smaller than the one of the NiFe/IrMn case. This smaller value is in good agreement with the fact that we do not observe a shift in the hysteresis loop due to real exchange bias, but an enlargement related to some pinning with uncompensated spins.

IV. CONCLUSION

In summary, we have investigated the temperature dependence of the dynamics of LSMO thin films, with thicknesses in the 5.6–16.5-nm range. This study has revealed that despite the half metallic nature of LSMO at low temperature, the damping is larger at 30 K than that at room temperature. We interpreted this temperature dependence considering resistive-like and conductive-like contributions, and an additional term due to spin pumping. This last term arises from the presence of an insulating and magnetically active dead layer, caused by the lowering of the double exchange mechanism at surface and interfaces. The coupling between the magnetic moments in the ferromagnetic metallic part of the LSMO layer and the spins of this magnetically active insulating layer, which have shorter spin relaxation time, alters the resonance field and leads to an increased damping. The presence of this magnetically active

dead layer, barely visible in quasistatic experiments such as SQUID magnetometry, is revealed by the surface/interface sensitive FMR technique through the peak appearing in the damping and the associated changes in the resonance field. This further highlights the potential of technics such as FMR to gain insight on the magnetic properties of heterostructures. The small damping of 2.63×10^{-3} at room temperature measured for the thicker films qualifies LSMO films as efficient sources of spin current. Furthermore, the opportunity to easily combine LSMO with other ferroelectric or multiferroic perovskites in multifunctional architecture opens new routes towards multifunctional devices such as artificial magnonic crystals [54].

ACKNOWLEDGMENTS

This work received support from the Projects OISO and CONTRABASS under Grant Agreements No. ANR-17-CE24-0026 and No. ANR-20-CE24-0023 from the Agence Nationale de la Recherche, the European Union's Horizon 2020 research and innovation program within the FET-OPEN project CHIRON under Grant Agreement No. 801055 and the project AXION, and the public grant overseen by the French National Research Agency (ANR) as part of the "Investissements d'Avenir" program (Labex NanoSaclay, Reference No. ANR-10-LABX-0035).

-
- [1] M. Bowen, M. Bibes, A. Barthélemy, J.-P. Contour, A. Anane, Y. Lemaître, and A. Fert, Nearly total spin polarization in $\text{La}_{2/3}\text{Sr}_{1/3}\text{MnO}_3$ from tunneling experiments, *Appl. Phys. Lett.* **82**, 233 (2003).
- [2] E. Lesne, Yu Fu, S. Oyarzun, J. C. Rojas-Sánchez, D. C. Vaz, H. Naganuma, G. Sicoli, J.-P. Attané, M. Jamet, E. Jacquet, J.-M. George, A. Barthélemy, H. Jaffrès, A. Fert, M. Bibes, and L. Vila, Highly efficient and tunable spin-to-charge conversion through Rashba coupling at oxide interfaces, *Nat. Mater.* **15**, 1261 (2016).
- [3] A. Ohtomo and H. Y. Hwang, A high-mobility electron gas at the $\text{LaAlO}_3/\text{SrTiO}_3$ heterointerface, *Nature (London)* **427**, 423 (2004).
- [4] J. T. Heron, J. L. Bosse, Q. He, Y. Gao, M. Trassin, L. Ye, J. D. Clarkson, C. Wang, Jian Liu, S. Salahuddin, D. C. Ralph, D. G. Schlom, J. Íñiguez, B. D. Huey, and R. Ramesh, Deterministic switching of ferromagnetism at room temperature using an electric field, *Nature (London)* **516**, 370 (2014).
- [5] P. Noël, F. Trier, L. M. V. Arche, J. Bréhin, D. C. Vaz, V. Garcia, S. Fusil, A. Barthélemy, L. Vila, M. Bibes, and J.-P. Attané, Non-volatile electric control of spin-charge conversion in a SrTiO_3 Rashba system, *Nature (London)* **580**, 483 (2020).
- [6] V. Garcia, S. Fusil, K. Bouzehouane, S. Enouz-Vedrenne, N. D. Mathur, A. Barthélemy, and M. Bibes, Giant tunnel electroresistance for non-destructive readout of ferroelectric states, *Nature (London)* **460**, 81 (2009).
- [7] M. Gajek, M. Bibes, S. Fusil, K. Bouzehouane, J. Fontcuberta, A. E. Barthélemy, and A. Fert, Tunnel Junctions with Multiferroic Barriers, *Nat. Mater.* **6**, 296 (2007).
- [8] V. Garcia, M. Bibes, L. Bocher, S. Valencia, F. Kronast, A. Crassous, X. Moya, S. Enouz-Vedrenne, A. Gloter, D. Imhoff, C. Deranlot, N. D. Mathur, S. Fusil, K. Bouzehouane, and A. Barthélemy, Ferroelectric control of spin polarization, *Science* **327**, 1106 (2010).
- [9] L. D. Landau and E. M. Lifshitz, On the theory of the dispersion of magnetic permeability in ferromagnetic bodies, *Phys. Z. Sowjetunion* **8**, 153 (1935).
- [10] T. L. Gilbert, A Lagrangian formulation of the gyromagnetic equation of the magnetization field, *Phys. Rev.* **100**, 1243 (1955).
- [11] C. Liu, C. K. A. Mewes, M. Chshiev, T. Mewes, and W. H. Butler, Origin of low Gilbert damping in half metals, *Appl. Phys. Lett.* **95**, 022509 (2009).
- [12] S. Andrieu, A. Neggache, T. Hauet, T. Devolder, A. Hallal, M. Chshiev, A. M. Bataille, P. Le Fèvre, and F. Bertran, Direct evidence for minority spin gap in the Co_2MnSi Heusler compound, *Phys. Rev. B* **93**, 094417 (2016); C. Guillemard, W. Zhang, G. Malinowski, C. de Melo, J. Gorchon, S. Petit-Watelot, J. Ghanbaja, S. Mangin, P. Le Fèvre, F. Bertran, and S. Andrieu, Engineering $\text{Co}_2\text{MnAl}_x\text{Si}_{1-x}$ Heusler compounds as a model system to correlate spin polarization, intrinsic Gilbert damping, and ultrafast demagnetization, *Adv. Mater.* **32**, 1908357 (2020).
- [13] J.-H. Park, E. Vescovo, H.-J. Kim, C. Kwon, R. Ramesh, and T. Venkatesan, Direct evidence for a half-metallic ferromagnet, *Nature (London)* **392**, 794 (1998).
- [14] Q. Qin, S. He, W. Song, P. Yang, Q. Wu, Y. P. Feng, and J. Cheng, Ultra-low magnetic damping of perovskite $\text{La}_{0.7}\text{Sr}_{0.3}\text{MnO}_3$ thin films, *Appl. Phys. Lett.* **110**, 112401 (2017).
- [15] B. Khodadadi, A. Rai, A. Sapkota, A. Srivastava, B. Nepal, Y. Lim, D. A. Smith, C. Mewes, S. Budhathoki, A. J. Hauser, M. Gao, J.-F. Li, D. D. Viehland, Z. Jiang, J. J. Heremans,

- P. V. Balachandran, T. Mewes, and S. Emori, Conductivitylike Gilbert Damping due to Intraband Scattering in Epitaxial Iron, *Phys. Rev. Lett.* **124**, 157201 (2020).
- [16] L. Frangou, G. Forestier, S. Auffret, S. Gambarelli, and V. Baltz, Relaxation mechanism in NiFe thin films driven by spin angular momentum absorption throughout the antiferromagnetic phase transition in native surface oxides, *Phys. Rev. B* **95** 054416 (2017).
- [17] O. Gladii, L. Frangou, G. Forestier, R. L. Seeger, S. Auffret, I. Joumard, M. Rubio-Roy, S. Gambarelli, and V. Baltz, Unraveling the influence of electronic and magnonic spin-current injection near the magnetic ordering transition of IrMn metallic antiferromagnets, *Phys. Rev. B* **98** 094422 (2018).
- [18] M. Ziese, H. C. Semmelhack, and P. Busch, Sign reversal of the magnetic anisotropy in $\text{La}_{0.7}\text{A}_{0.3}\text{MnO}_3$ ($\text{A} = \text{Ca}, \text{Sr}, \text{Ba}, \square$) films, *J. Magn. Magn. Mater.* **246**, 327 (2002).
- [19] J. Z. Sun and D. W. Abraham, Thickness-dependent magnetotransport in ultrathin manganite films, *Appl. Phys. Lett.* **74**, 3017 (1999).
- [20] M. Huijben, L. W. Martin, Y.-H. Chu, M. B. Holcomb, P. Yu, G. Rijnders, D. H. A. Blank, and R. Ramesh, Critical thickness and orbital ordering in ultrathin $\text{La}_{0.7}\text{Sr}_{0.3}\text{MnO}_3$ films, *Phys. Rev. B* **78**, 094413 (2008).
- [21] J. Choi, J. Zhang, S.-H. Liou, P. A. Dowben, and E. W. Plummer, Surfaces of the perovskite manganites $\text{La}_{1-x}\text{Ca}_x\text{MnO}_3$, *Phys. Rev. B* **59**, 13453 (1999); H. Dulli, P. A. Dowben, S.-H. Liou, and E. W. Plummer, Surface segregation and restructuring of colossal-magnetoresistant manganese perovskites $\text{La}_{0.65}\text{Sr}_{0.35}\text{MnO}_3$, *ibid.* **62**, R14629(R) (2000).
- [22] M. Bibes, Ll. Balcells, S. Valencia, J. Fontcuberta, M. Wojcik, E. Jedryka, and S. Nadolski, Nanoscale Multiphase Separation at $\text{La}_{2/3}\text{Ca}_{1/3}\text{MnO}_3/\text{SrTiO}_3$ Interfaces, *Phys. Rev. Lett.* **87**, 067210 (2001).
- [23] M. P. de Jong, I. Bergenti, V. A. Dediu, M. Fahlman, M. Marsi, and C. Taliani, Evidence for Mn^{2+} ions at surfaces of $\text{La}_{0.7}\text{Sr}_{0.3}\text{MnO}_3$ thin films, *Phys. Rev. B* **71**, 014434 (2005).
- [24] D. Pesquera, G. Herranz, A. Barla, E. Pellegrin, F. Bondino, E. Magnano, F. Sánchez, and J. Fontcuberta, Surface symmetry-breaking and strain effects on orbital occupancy in transition metal perovskite epitaxial films, *Nat. Commun.* **3**, 1189 (2012); S. Valencia, L. Peña, Z. Konstantinovic, L. Balcells, R. Galceran, D. Schmitz, F. Sandiumenge, M. Casanove, and B. Martínez, Intrinsic antiferromagnetic/insulating phase at manganite surfaces and interfaces, *J. Phys.: Condens. Matter* **26**, 166001 (2014).
- [25] Note that it is not possible to take into account finite size effects in a Fuchs Sondheimer approach since the mean free path calculated considering the resistivity values (1.1 nm for the 5.6-nm film and 5.3 nm for the 16.5 nm one) are of the same order as the film thicknesses.
- [26] M. Angeloni, G. Balestrino, N. G. Boggio, P. G. Medaglia, P. Orgiani, and A. Tebano, Suppression of the metal-insulator transition temperature in thin $\text{La}_{0.7}\text{Sr}_{0.3}\text{MnO}_3$ films, *J. Appl. Phys.* **96**, 6387 (2004).
- [27] C. Kittel, On the theory of ferromagnetic resonance absorption, *Phys. Rev.* **73**, 155 (1948).
- [28] S. Emori, U. S. Alaani, M. T. Gray, V. Sluka, Y. Chen, A. D. Kent, and Y. Suzuki, Spin transport and dynamics in all-oxide perovskite $\text{La}_{2/3}\text{Sr}_{1/3}\text{MnO}_3/\text{SrRuO}_3$ bilayers probed by ferromagnetic resonance, *Phys. Rev. B* **94** 224423 (2016).
- [29] V. Flovik, F. Macià, S. Lendínez, Jo. M. Hernández, I. Hallsteinsen, T. Tybell, and E. Wahlström, Thickness and temperature dependence of the magnetodynamic damping of pulsed laser deposited $\text{La}_{0.7}\text{Sr}_{0.3}\text{MnO}_3$ on (111)-oriented SrTiO_3 , *J. Magn. Magn. Mater.* **420**, 280 (2016).
- [30] G. Y. Luo, M. Belmeguenai, Y. Roussigné, C. R. Chang, J. G. Lin, and S. M. Chérif, Enhanced magnetic damping in $\text{La}_{0.7}\text{Sr}_{0.3}\text{MnO}_3$ capped by normal metal layer, *AIP Adv.* **5**, 097148 (2015).
- [31] M. A. W. Schoen, D. Thonig, M. L. Schneider, T. J. Silva, H. T. Nembach, O. Eriksson, O. Karis, and J. M. Shaw, Ultra-low magnetic damping of a metallic ferromagnet, *Nat. Phys.* **12**, 839 (2016); T. Devolder, T. Tahmasebi, S. Eimer, T. Hauet, and S. Andrieu, Compositional dependence of the magnetic properties of epitaxial FeV/MgO thin films, *Appl. Phys. Lett.* **103**, 242410 (2013).
- [32] A. Conca, A. Niesen, G. Reiss, and B. Hillebrands, Low damping magnetic properties and perpendicular magnetic anisotropy in the Heusler alloy $\text{Fe}_{1.5}\text{CoGe}$, *AIP Adv.* **9**, 085205 (2019).
- [33] H. K. Lee, I. Barsukov, A. G. Swartz, B. Kim, L. Yang, H. Y. Hwang, and I. N. Krivorotov, Magnetic anisotropy, damping, and interfacial spin transport in Pt/LSMO bilayers, *AIP Adv.* **6**, 055212 (2016).
- [34] M. Strungaru, S. Ruta, R. F. L. Evans, and R. W. Chantrell, Model of Magnetic Damping and Anisotropy at Elevated Temperatures: Application to Granular FePt Films, *Phys. Rev. Appl.* **14**, 014077 (2020).
- [35] C. L. Jermain, S. V. Aradhya, N. D. Reynolds, R. A. Buhrman, J. T. Brangham, M. R. Page, P. C. Hammel, F. Y. Yang, and D. C. Ralph, Increased low-temperature damping in yttrium iron garnet thin films, *Phys. Rev. B* **95**, 174411 (2017).
- [36] G. Malinowski, K. C. Kuiper, R. Lavrijsen, H. J. M. Swagten, and B. Koopmans, Magnetization dynamics and Gilbert damping in ultrathin $\text{Co}_{48}\text{Fe}_{32}\text{B}$ films with out-of-plane anisotropy, *Appl. Phys. Lett.* **94**, 102501 (2009).
- [37] B. Heinrich, Spin relaxation in magnetic metallic layers, and multilayers, in *Ultrathin Magnetic Structures III*, edited by J. A. C. Bland and B. Heinrich (Springer-Verlag, Berlin, 2005), pp. 143–210.
- [38] B. Heinrich, D. J. Meredith, and J. F. Cochran, Wave number and temperature dependent Landau-Lifshitz damping in nickel, *J. Appl. Phys.* **50**, 7726 (1979).
- [39] V. Kamberský, On ferromagnetic resonance damping in metals, *Czech. J. Phys. B* **26**, 1366 (1976).
- [40] K. Gilmore, Y. U. Idzerda, and M. D. Stiles, Identification of the Dominant Precession-Damping Mechanism in Fe, Co, and Ni by First-Principles Calculations, *Phys. Rev. Lett.* **99**, 027204 (2007).
- [41] J.-H. Park, E. Vescovo, H.-J. Kim, C. Kwon, R. Ramesh, and T. Venkatesan, Magnetic Properties at Surface Boundary of a Half-Metallic Ferromagnet $\text{La}_{0.7}\text{Sr}_{0.3}\text{MnO}_3$, *Phys. Rev. Lett.* **81**, 1953 (1998).
- [42] M. Cyrot, Theory of Mott transition: Application to transition metal oxides, *J. Phys.* **33**, 125 (1972).
- [43] C. Hauser, C. Ballani, P. Dürrenfeld, F. Heyroth, P. Trempler, S. G. Ebbinghaus, E. Th. Papaioannou, and G. Schmidt, Enhancement of spin mixing conductance in $\text{La}_{0.7}\text{Sr}_{0.3}\text{MnO}_3/\text{LaNiO}_3/\text{SrRuO}_3$ heterostructures, *Phys. Status Solidi B* **257**, 1900606 (2020).

- [44] M. Wahler, N. Homonnay, T. Richter, A. Müller, C. Eischmidt, B. Fuhrmann, and G. Schmidt, Inverse spin Hall effect in a complex ferromagnetic oxide heterostructure, *Sci. Rep.* **6**, 28727 (2016).
- [45] D. C. Vaz, P. Noël, A. Johansson, B. Göbel, F. Y. Bruno, G. Singh, S. McKeown-Walker, F. Trier, L. M. Vicente-Arche, A. Sander, S. Valencia, P. Bruneel, M. Vivek, M. Gabay, N. Bergeal, F. Baumberger, H. Okuno, A. Barthélémy, A. Fert, L. Vila *et al.*, Mapping spin–charge conversion to the band structure in a topological oxide two-dimensional electron gas, *Nat. Mater.* **18**, 1187 (2019).
- [46] O. Gladii, L. Frangou, G. Forestier, R. Lopes Seeger, S. Auffret, M. Rubio-Roy, R. Weil, A. Mougin, C. Gomez, W. Jahjah, J.-P. Jay, D. Dekadjevi, D. Spenato, S. Gambarelli, and V. Baltz, Spin pumping as a generic probe for linear spin fluctuations: Demonstration with ferromagnetic and antiferromagnetic orders, metallic and insulating electrical states, *Appl. Phys. Express* **12**, 023001 (2019).
- [47] J. Nogues, J. Sort, V. Langlais, V. Skurmyev, S. Suriñach, J. S. Muñoz, and M. D. Baro, Exchange bias in nanostructures, *Phys. Rep.* **422**, 65 (2005).
- [48] H. Yamada, Y. Ogawa, Y. Ishii, H. Sato, M. Kawasaki, H. Akoh, and Y. Tokura, Engineered interface of magnetic oxides, *Science* **305**, 646 (2004).
- [49] M. Izumi, Y. Ogimoto, Y. Okimoto, T. Manako, P. Ahmet, K. Nakajima, T. Chikyow, M. Kawasaki, and Y. Tokura, Insulator-metal transition induced by interlayer coupling in $\text{La}_{0.6}\text{Sr}_{0.4}\text{MnO}_3/\text{SrTiO}_3$ superlattices, *Phys. Rev. B* **64**, 064429 (2001).
- [50] X. Li, I. Lindfors-Vrejoiu, M. Ziese, A. Gloter, and P. A. van Aken, Impact of interfacial coupling of oxygen octahedra on ferromagnetic order in $\text{La}_{0.7}\text{Sr}_{0.3}\text{MnO}_3/\text{SrTiO}_3$ heterostructures, *Sci. Rep.* **7**, 40068 (2017).
- [51] K. Dörr, T. Walter, M. Sahana, K.-H. Müller, K. Nenkov, and L. Schultz, Magnetotransport of $\text{La}_{0.7}\text{Sr}_{0.3}\text{MnO}_3/\text{SrTiO}_3$ multilayers with ultrathin manganite layers, *J. Appl. Phys.* **89**, 6973 (2001).
- [52] R. P. Borges, W. Guichard, J. G. Lunney, and J. M. D. Coey, and F. Ott, Magnetic and electric “dead” layers in $\text{La}_{0.7}\text{Sr}_{0.3}\text{MnO}_3$ thin films, *J. Appl. Phys.* **89**, 3868 (2001).
- [53] J. McCord, R. Mattheis, and D. Elefant, Dynamic magnetic anisotropy at the onset of exchange bias: The NiFe/IrMn ferromagnet/antiferromagnet system, *Phys. Rev. B* **70**, 094420 (2004).
- [54] H. Merbouche, I. Boventer, V. Haspot, S. Fusil, V. Garcia, D. Gouéré, C. Carrétéro, A. Vecchiola, P. Bortolotti R. Lebrun, L. Vila, M. Bibes, A. Barthélémy, and A. Anane, Voltage-controlled reconfigurable magnonic crystal at the sub-micrometer scale, *ACS Nano* **15**, 9775 (2021).